Inorganic Chemistry

Article

pubs.acs.org/IC

Electrochemically Directed Synthesis of $Cu_2^{I}(TCNQF_4^{II-})(MeCN)_2$ ($TCNQF_4$ = 2,3,5,6-Tetrafluoro-7,7,8,8-tetracyanoquinodimethane): Voltammetry, Simulations, Bulk Electrolysis, Spectroscopy, Photoactivity, and X-ray Crystal Structure of the $Cu_2^{I}(TCNQF_4^{II-})(EtCN)_2$ Analogue

Thanh H. Le,[†,¶] Ayman Nafady,[†,§] Nguyen T. Vo,[†] Robert W. Elliott,[‡] Timothy A. Hudson,[‡] Richard Robson,[‡] Brendan F. Abrahams,[‡] Lisandra L. Martin,*[,†] and Alan M. Bond*[,†]

[†]School of Chemistry, Monash University, Clayton, Victoria 3800, Australia

[‡]School of Chemistry, The University of Melbourne, Parkville, 3001, Victoria, Australia

Supporting Information

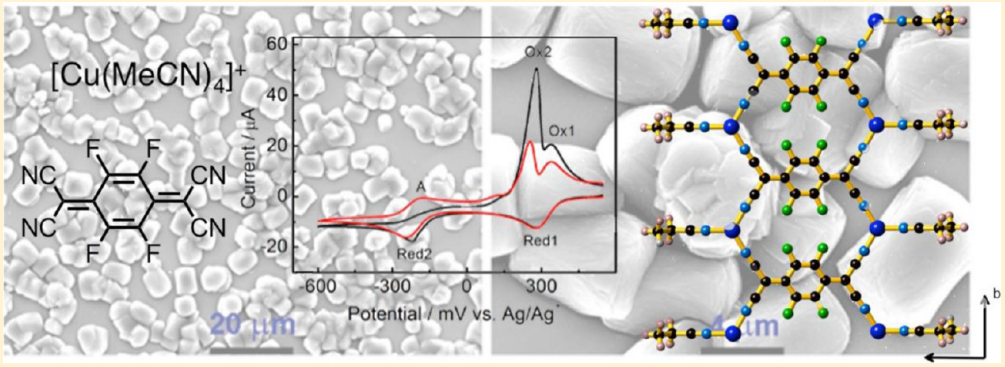

ABSTRACT: The new compound $Cu_2^{I}(TCNQF_4^{II-})(MeCN)_2$ ($TCNQF_4^{2-}$ = dianion of 2,3,5,6-tetrafluoro-7,7,8,8-tetracyanoquinodimethane) has been synthesized by electrochemically directed synthesis involving reduction of $TCNQF_4$ to $TCNQF_4^{2-}$ in acetonitrile containing $[Cu(MeCN)_4]^+_{(MeCN)}$ and 0.1 M Bu_4NPF_6. In one scenario, $TCNQF_4^{2-}$ is quantitatively formed by reductive electrolysis of $TCNQF_4$ followed by addition of $[Cu(MeCN)_4]^+$ to form the $Cu_2^{I}(TCNQF_4^{II-})(MeCN)_2$ coordination polymer. In a second scenario, $TCNQF_4$ is reduced in situ at the electrode surface to $TCNQF_4^{2-}$, followed by reaction with the $[Cu(MeCN)_4]^+$ present in the solution, to electrocrystallize $Cu_2^{I}(TCNQF_4^{II-})(MeCN)_2$. Two distinct phases of $Cu_2^{I}(TCNQF_4^{II-})(MeCN)_2$ are formed in this scenario; the kinetically favored form being rapidly converted to the thermodynamically favored $Cu_2^{I}(TCNQF_4^{II-})(MeCN)_2$. The postulated mechanism is supported by simulations. The known compound $Cu^{I}TCNQF_4^{I-}$ also has been isolated by one electron reduction of $TCNQF_4$ and reaction with $[Cu(MeCN)_4]^+$. The solubility of both $TCNQF_4^{2-}$- and $TCNQF_4^{\bullet-}$-derived solids indicates that the higher solubility of $Cu^{I}TCNQF_4^{I-}$ prevents its precipitation, and thus $Cu_2^{I}(TCNQF_4^{II-})(MeCN)_2$ is formed. UV−visible and vibrational spectroscopies were used to characterize the materials. $Cu_2^{I}(TCNQF_4^{II-})(MeCN)_2$ can be photochemically transformed to $Cu^{I}TCNQF_4^{I-}$ and Cu^0. Scanning electron microscopy images reveal that $Cu^{I}TCNQF_4^{I-}$ and $Cu_2^{I}(TCNQF_4^{II-})(MeCN)_2$ are electrocrystallized with distinctly different morphologies. Thermogravimetric and elemental analysis data confirm the presence of CH_3CN, and single-crystal X-ray diffraction data for the $Cu_2^{I}(TCNQF_4^{II-})(EtCN)_2$ analogue shows that this compound is structurally related to $Cu_2^{I}(TCNQF_4^{II-})(MeCN)_2$.

1. INTRODUCTION

Organic charge-transfer complexes containing conjugated (π-electron) ligands and transition metals have been widely investigated[1−3] because of their technologically important optical, electrical, and magnetic properties.[2,4,5] Of relevance to the present studies, it is noted that transition metal−organic charge-transfer TCNQ-based materials (TCNQ = 7,7,8,8-tetracyanoquinodimethane, Figure 1a) have been of considerable interest in energy and data storage,[6,7] optical and electrical media recording,[8] catalysis,[9−11] light-emitting, magnetic, and sensor device applications.[8,12−14] In those applications charge transfer is derived from Cu^{I}−$TCNQ^{I-}$ interaction in $Cu^{I}TCNQ^{I-}$. Now attention has been drawn to nanocrystals that have the composition ratio of 1.3:1 and contain both the $TCNQ^{\bullet-}$ anion radical and dianion.[15]

Received: January 29, 2014
Published: February 25, 2014

   dx.doi.org/10.1021/ic500225v | *Inorg. Chem.* 2014, 53, 3230−3242

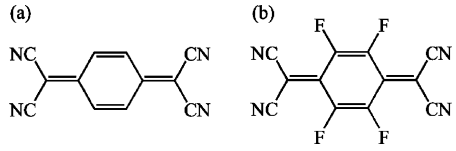

Figure 1. Molecular structures of (a) TCNQ and (b) $TCNQF_4$.

Recently, a series of studies has focused on the synthesis, structure, magnetic properties, and optically induced transformation of the tetraflouro $TCNQF_4^{\bullet-}$-based materials ($TCNQF_4$ = 2,3,5,6-tetrafluoro-7,7,8,8-tetracyanoquinodimethane, Figure 1b).[2,16−21] For example, $Ag^ITCNQF_4^{I-}$ and $Cu^ITCNQF_4^{I-}$ exhibit electrical switching phenomena, memory storage capability,[22] and are potential candidates for use in reversible bistable electrical and optical switches, memory effects,[2,22] and field-emission cathodes.[18] $TCNQF_4$ is a far stronger electron acceptor than TCNQ with the reversible formal potentials associated with generation of the anion radical and dianion in acetonitrile (0.1 M Bu_4NClO_4) being 0.36 and 0.37 V more positive, respectively.[23] Thus the introduction of fluorine substituents leads to enhanced stability of both the anion radical $TCNQF_4^{\bullet-}$ and the dianion $TCNQF_4^{2-}$,[23] which is of interest in this Study.

$Cu^ITCNQF_4^{I-}$ has been chemically synthesized by controlling the temperature for the reaction of $TCNQF_4$ powder and Cu foil in a ceramic boat[18] or by placing a polished Cu metal substrate in a dry and degassed saturated acetonitrile solution of $TCNQF_4$.[22] A series of stable crystallographically characterized compounds of composition $A[Cu^I(TCNQF_4^{II-})]$, where A = a quaternary ammonium or phosphonium, also have been reported.[24] These $TCNQF_4^{2-}$ derivatives were synthesized by reaction of $[Cu(MeCN)_4]^+$ and H_2TCNQF_4 under mildly basic conditions. In the present study, $Cu^ITCNQF_4^{I-}$ and the new material $Cu_2^I(TCNQF_4^{II-})(MeCN)_2$ have been synthesized by mixing an acetonitrile solution of $[Cu(MeCN)_4]^+$ with air stable $TCNQF_4^{\bullet-}$ or $TCNQF_4^{2-}$ in acetonitrile, which were electrochemically generated by bulk reductive electrolysis of $TCNQF_4$ in acetonitrile (0.1 M Bu_4NPF_6) at a Pt foil electrode. Electrochemically directed methods also have been used to electrocystallize $Cu^ITCNQF_4^{I-}$ and $Cu_2^I(TCNQF_4^{II-})(MeCN)_2$ onto an electrode surface. Thus, $TCNQF_4$ present in acetonitrile (0.1 M Bu_4NPF_6) solution containing $[Cu(MeCN)_4]^+$ is reduced to $TCNQF_4^{\bullet-}$ or $TCNQF_4^{2-}$ to deposit $Cu^ITCNQF_4^{I-}$ or $Cu_2^I(TCNQF_4^{II-})(MeCN)_2$, respectively, onto the electrode surface under carefully selected conditions. Electrocrystallization can only occur when the solubility products of $Cu^ITCNQF_4^{I-}$ or $Cu_2^I(TCNQF_4^{II-})(MeCN)_2$ are exceeded, so a knowledge of these parameters and reactant concentrations along with control of electrochemical conditions is required. $Cu^ITCNQF_4^{I-}$ and $Cu_2^I(TCNQF_4^{II-})(MeCN)_2$ synthesized electrochemically have been characterized by ultraviolet−visible (UV−vis), Fourier transform infrared (FT-IR), and Raman spectroscopies. Scanning electron microscopy (SEM) images of electrode surfaces were used to define the morphology of the electrocrystallized materials. Electrochemically generated $TCNQF_4^{2-}$ is seen to provide a more facile route to the synthesis of dianion-based derivatives of $TCNQ^{2-}$ where instability associated with aerial oxidation provides difficulties.[25−27] The structure of $Cu_2^I(TCNQF_4^{II-})(MeCN)_2$ is assumed to be the same as that determined by X-ray crystallography for $Cu_2^I(TCNQF_4^{II-})(EtCN)_2$, which was synthesized chemically from H_2TCNQF_4 using the method developed for preparation of $A[Cu^I(TCNQF_4^{II-})]$. Unfortunately, no crystal suitable for X-ray structural analysis could be obtained for the MeCN derivative.

2. EXPERIMENTAL METHODS

2.1. Chemicals. $[Cu(MeCN)_4]PF_6$ (98%, Aldrich), $TCNQF_4$ (98%, Beijing Health), acetonitrile (HPLC grade, Omnisolv or Ajax Finechem), isopropanol (BDH), acetone (Suprasolv, Merck KGaA), methanol (Chem Supply), propionitrile (Aldrich), dimethyl sulfoxide (DMSO) (Chem Supply), and lithium acetate (Sigma Aldrich) were used as received from the manufacturer. Bu_4NPF_6 (Wako), used as the supporting electrolyte in voltammetric and electrodeposition studies, was recrystallized twice from 96% ethanol (Merck) and then dried at 100 °C under vacuum for 24 h. H_2TCNQF_4 and $[Cu(MeCN)_4]ClO_4$ was prepared according to the literature methods.[28,29]

2.2. Synthesis. $Cu^ITCNQF_4^{I-}$ was prepared in bulk quantities by reaction of electrochemically generated $TCNQF_4^{\bullet-}$ and $[Cu(MeCN)_4]^+$ in acetonitrile. Thus, 5.0 mL of 5.0 mM $TCNQF_4^{\bullet-}$ was quantitatively prepared by electrochemical reduction of 5.0 mM $TCNQF_4$ in acetonitrile (0.1 M Bu_4NPF_6) with the potential of the Pt foil working electrode held at 100 mV versus Ag/Ag^+, which lies between the $TCNQF_4^{0/\bullet-}$ and $TCNQF_4^{\bullet-/2-}$ processes. The $TCNQF_4^{\bullet-}$ solution was then mixed with 0.25 mL of 100 mM $[Cu(MeCN)_4]^+$ in acetonitrile. The black precipitate that immediately formed was collected and washed with 4 × 2 mL of acetonitrile. The solid was used directly for determination of the solubility of $Cu^ITCNQF_4^{I-}$ in acetonitrile or dried under vacuum overnight before spectroscopic characterization (see Section 3).

Electrochemical synthesis of $Cu_2^I(TCNQF_4^{II-})(MeCN)_2$ was achieved in an analogous manner to that for $Cu^ITCNQF_4^{I-}$. However, in this case, reaction of 2.0 mL of 5.0 mM $TCNQF_4^{2-}$ (synthesized by exhaustive reductive electrolysis at a platinum foil electrode of $TCNQF_4^{\bullet-}$ in acetonitrile (0.1 M Bu_4NPF_6) at −400 mV versus Ag/Ag^+) and 0.20 mL of 100 mM $[Cu(MeCN)_4]^+$ in acetonitrile was used. $Cu_2^I(TCNQF_4^{II-})(MeCN)_2$ precipitated and was collected as a white microcrystalline solid.

The chemical synthesis of $Cu^I(TCNQF_4^{II-})(EtCN)_2$ employed $[Cu(MeCN)_4]ClO_4$ (15.3 mg, 0.047 mmol), which was dissolved in EtCN (1.0 mL). The resulting solution was mixed with a solution of $Li(OAc)\cdot 2H_2O$ (82.5 mg, 0.81 mmol) in MeOH (4.0 mL) under a nitrogen atmosphere. The solution was then allowed to slowly diffuse into a solution of H_2TCNQF_4 (13 mg, 0.047 mmol) in DMSO (1.0 mL). Crystals suitable for single-crystal analysis were transferred directly from the mother liquor to a protective oil prior to structural analysis.

2.3. Electrochemistry. Voltammetric experiments were undertaken at room temperature (22 ± 2 °C) with a Bioanalytical Systems (BAS) 100 W electrochemical workstation using a standard three-electrode cell configuration. Working electrodes (WEs) were BAS glassy carbon (GC, 3.0 mm diameter), gold or platinum (1.6 mm diameter) disks, carbon fiber microelectrode (11 ± 2 μm diameter as quoted), or indium tin oxide (ITO)-coated glass plates (0.1−0.2 cm^2) with a resistance of 10 Ω/sq, as specified by the manufacturer (Prazisions Glas and Optik GmbH). The procedures for polishing the WEs are as reported previously.[30] A Ag wire in contact with acetonitrile containing 1.0 mM $AgNO_3$ and 0.1 M Bu_4NPF_6, separated from the test solution by a salt bridge, was used as a reference electrode (the potential of this reference electrode is −135 ± 5 mV versus the ferrocene/ferrocenium couple, $Fc^{0/+}$). The counter electrode was a 1.0 mm diameter platinum wire. Solutions used in voltammetric studies were purged with nitrogen gas for 10 min, and a stream of nitrogen was then maintained above the solutions during the course of the experiments. Bulk electrolysis and in situ surface plasmon resonance (SPR) studies used a Pt foil and a gold film coated on a glass plate, respectively, as working electrodes; the reference and counter electrodes have been described previously.[30] Electrochemical quartz crystal microbalance (EQCM) experiments were undertaken with an ELCHEMA EQCN-701 quartz crystal microbalance and a PS-205 potentiostat connected to a computer via an Advantech PCI-1711

dx.doi.org/10.1021/ic500225v | Inorg. Chem. 2014, 53, 3230−3242

DAQ device. In this case, a 5.0 mm diameter Au electrode, formed as a film on 1.3 cm diameter quartz crystal, was used as the working electrode, Ag/Ag^+ as the reference electrode, and Pt wire as the counter electrode. Simulation software DigiElch 6.F distributed by Gamry Instruments was used to simulate cyclic voltammograms.

2.4. Crystallography. $[Cu_2(TCNQF_4)(EtCN)_2]$, Formula: $C_{18}H_{10}Cu_2F_4N_6$; FW 513.40; crystal system monoclinic; space group *I2/m*; pale yellow; cell dimensions a = 10.0785(6), b = 7.5317(3), c = 12.8559(8) Å, β = 110.743(7)°; V = 912.61(9) Å^3, T = 130 K; Z = 2; $wR2$ (all data) = 0.0801; $R1$ ($I > 2\sigma(I)$) = 0.0285; GOF = 1.119. Data were collected on an Oxford Diffraction Supernova diffractometer. The structure was solved using direct methods and refined using a full-matrix least-squares procedure, using all data,[31] within the WinGX program system.[32] The X-ray powder diffraction (XRD) pattern of $Cu_2^{I}(TCNQF_4^{II-})(MeCN)_2$ also was collected using the Oxford Diffraction Supernova diffractometer.

2.5. Other Instrumentation. Instrumentation used in UV−vis, FT-IR, and Raman spectroscopic experiments, SEM imaging, and energy dispersive X-ray spectroscopy (EDXS) analysis is as described previously.[30,33] Thermogravimetric analysis (TGA) was undertaken under a stream of dry nitrogen gas (30 mL min^{-1}) over the temperature range from 25 to 350 °C at a rate of 5 °C min^{-1}, using aluminum pans and a Mettler-Toledo model TGA-DSC1 instrument. The reported TGA data was deduced after subtraction of the blank data (obtained with an empty aluminum pan) from the raw data (obtained with the aluminum pan containing the material being studied).

3. RESULTS AND DISCUSSION

3.1. Electrocrystallization of $Cu^{I}TCNQF_4^{II-}$ and $Cu_2^{I}(TCNQF_4^{II-})(MeCN)_2$. The electrochemical experiments themselves do not provide evidence of the chemical composition of products formed by electrocrystallization. However, the products have been characterized as $Cu^{I}TCNQF_4^{I-}$ and $Cu_2^{I}(TCNQF_4^{II-})(MeCN)_2$ spectroscopically (as described below), and for convenience these formulations are used in the following discussion of the electrochemistry.

3.1.1. Voltammetry of $TCNQF_4$ and $[Cu(MeCN)_4]^+$ in Acetonitrile. A cyclic voltammogram for the reduction of 1.0 mM $TCNQF_4$ to $TCNQF_4^{\bullet-}$ and then to $TCNQF_4^{2-}$ (eqs 1 and 2) in acetonitrile (0.1 M Bu_4NPF_6) at a GC electrode is shown in Figure 2a. These $TCNQF_4^{0/\bullet-}$ and $TCNQF_4^{\bullet-/2-}$ redox couples both represent ideal reversible diffusion controlled one-electron processes.[34] In contrast, the cyclic voltammetry of $[Cu(MeCN)_4]^+$ is more complex, as shown in Figure 2b. Here on scanning the potential in the negative direction, $[Cu(MeCN)_4]^+$ (2.0 mM) is reduced to metallic Cu, which deposits onto the electrode surface. On scanning back in the positive potential direction, a sharp and large Cu stripping peak is detected. At a much more positive potential, the oxidation of $Cu^+_{(MeCN)}$ to $Cu^{2+}_{(MeCN)}$ occurs. However, the potentials for both the reduction and oxidation of $Cu^+_{(MeCN)}$ are well-removed from the reductions of $TCNQF_4$ to $TCNQF_4^{\bullet-}$ and $TCNQF_4^{\bullet-}$ to $TCNQF_4^{2-}$ (Table 1).

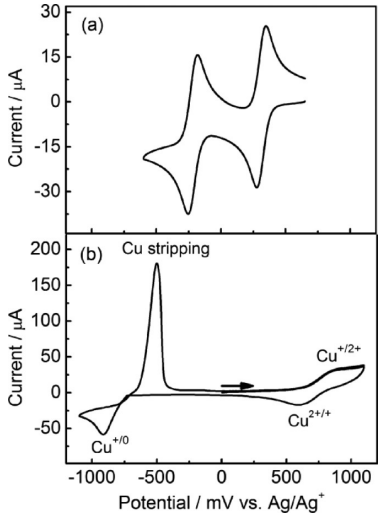

Figure 2. Cyclic voltammograms for (a) 1.0 mM $TCNQF_4$ and (b) 2.0 mM $Cu(MeCN)_4^+$ in acetonitrile (0.1 M Bu_4NPF_6) obtained with a 3.0 mm diameter GC electrode at a scan rate of 100 mV s^{-1}.

Table 1. Midpoint Potentials (E_m)[a,b] Derived from Cyclic Voltammograms Obtained for 1.0 mM $TCNQF_4$ and 2.0 mM $[Cu(MeCN)_4]^+$ in Separate Acetonitrile (0.1 M Bu_4NPF_6) Solutions at GC, Au, Pt, and ITO Electrodes

	process			
working electrode	$TCNQF_4^{0/\bullet-}$	$TCNQF_4^{\bullet-/2-}$	$Cu^{+/0}$	$Cu^{+/2+}$
GC	311	−220	−706	748
Au	310	−220	−630	560
Pt	310	−221	−659	545
ITO	304	−246	−640	725

[a]Midpoint potential is the average of the reduction E_p^{red} and oxidation E_p^{ox} peak potentials for a redox couple, i.e., $E_m = (E_p^{red} + E_p^{ox})/2$. [b]Potentials in mV vs Ag/Ag^+.

Consequently, the electrocrystallizations of $Cu^{I}TCNQF_4^{I-}{}_{(s)}$ (via eqs 1 and 3) and $Cu_2^{I}(TCNQF_4^{II-})(MeCN)_{2(s)}$ (via eqs 1, 2, and 4) via reduction of $TCNQF_4$ in acetonitrile (0.1 M Bu_4NPF_6) in the presence of $Cu^+_{(MeCN)}$ are possible in the region between the reduction and oxidation of $Cu^+_{(MeCN)}$. Nevertheless, electrocrystallization of $Cu_2TCNQF_{4(s)}$ will require discrimination against formation of $Cu^{I}TCNQF_4^{I-}$ if the reaction sequence 1, 2, and 4 is to be employed.

$$TCNQF_{4(MeCN)} + e^- \rightleftharpoons TCNQF_{4(MeCN)^{\bullet-}} \quad (1)$$

$$TCNQF_{4(MeCN)^{\bullet-}} + e^- \rightleftharpoons TCNQF_{4(MeCN)^{2-}} \quad (2)$$

$$Cu^+_{(MeCN)} + TCNQF_{4(MeCN)^{\bullet-}} \rightleftharpoons Cu^{I}TCNQF_{4(s)}{}^{I-} \quad (3)$$

$$2Cu^+_{(MeCN)} + TCNQF_{4(MeCN)^{2-}} \rightleftharpoons Cu_2^{I}(TCNQF_4^{II-})(MeCN)_{2(s)} \quad (4)$$

3.1.2. Electrocrystallization of $Cu^{I}TCNQF_4^{I-}{}_{(s)}$ and $Cu_2^{I}(TCNQF_4^{II-})(MeCN)_{2(s)}$ in Acetonitrile (0.1 M Bu_4NPF_6) Containing $TCNQF_4$ and $[Cu(MeCN)_4]^+$. (a). $Cu^{I}TCNQF_4^{I-}{}_{(s)}$. Figure 3 shows cyclic voltammograms derived from acetonitrile (0.1 M Bu_4NPF_6) solutions containing 10.0 mM $[Cu(MeCN)_4^+]$ and 1.0, 5.0, or 10.0 mM $TCNQF_4$ in acetonitrile (0.1 M Bu_4NPF_6), using a GC electrode at a scan rate of 20 mV s^{-1}. The potential was switched at 50 mV (vs Ag/Ag^+) to ensure $TCNQF_4$ was reduced to $TCNQF_4^{\bullet-}$ rather than $TCNQF_4^{2-}$. The cyclic voltammogram, with 1.0 mM $TCNQF_4$ present, retains the fully diffusion-controlled process associated with the $TCNQF_4^{0/\bullet-}$ couple (Figure 3a). When the concentration of $TCNQF_4$ is increased to 10.0 mM, the oxidation and reduction peak current ratio (i_p^{ox}/i_p^{red}) decreases from unity to ∼0.70. A loss of $TCNQF_4^{\bullet-}{}_{(MeCN)}$ and hence a decrease in oxidation peak current is as expected if the reduction of $TCNQF_4$ to $TCNQF_4^{\bullet-}$ is followed by rapid

dx.doi.org/10.1021/ic500225v | Inorg. Chem. 2014, 53, 3230−3242

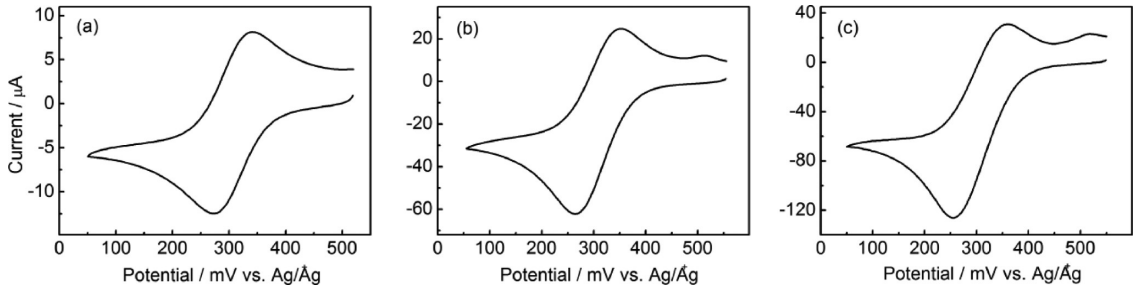

Figure 3. Cyclic voltammograms for acetonitrile (0.1 M Bu_4NPF_6) solutions containing 10.0 mM $[Cu(MeCN)_4]^+$ and (a) 1.0, (b) 5.0, and (c) 10.0 mM $TCNQF_4$, using a 3.0 mm diameter GC electrode (ν = 20 mV s^{-1}).

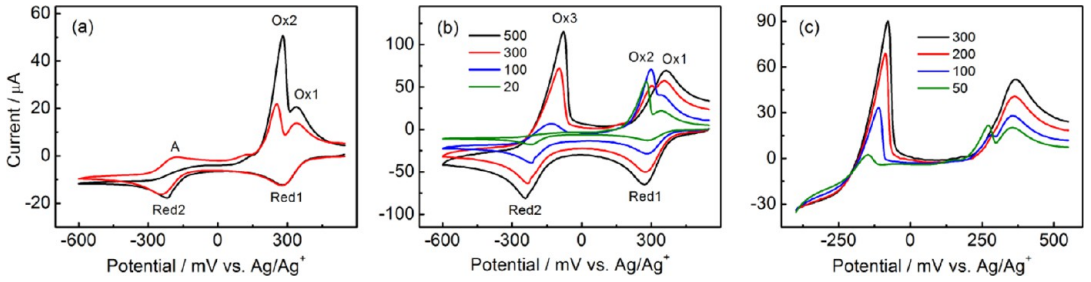

Figure 4. Voltammograms obtained with a 3.0 mm diameter GC electrode in acetonitrile (0.1 M Bu_4NPF_6) solutions containing (a) 1.0 mM $TCNQF_4$ in the presence of (black curve) 2.0 mM $[Cu(MeCN)_4]^+$ or (red curve) 1.0 mM $[Cu(MeCN)_4]^+$ at a scan rate of 20 mV s^{-1}; A refers to phase A discussed in the text, (b) 1.0 mM $TCNQF_4$ and 2.0 mM $[Cu(MeCN)_4]^+$ at designated scan rates (mV s^{-1}), and (c) under conditions as (b) but the potential was held at −400 mV for 1 s and then scanned in positive direction at designated scan rates (mV s^{-1}). All data were obtained with a 3.0 mm diameter GC electrode.

formation of $Cu^{I}TCNQF_4^{I-}{}_{(s)}$. However, electrocrystallization of $Cu^{I}TCNQF_4^{I-}{}_{(s)}$ may only occur under conditions where the concentration product of $TCNQF_4$ and $[Cu(MeCN)_4]^+$ exceeds the solubility product of $Cu^{I}TCNQF_4^{I-}{}_{(s)}$ in acetonitrile. Apparently, electrocrystallized $Cu^{I}TCNQF_4^{I-}{}_{(s)}$ is oxidized when the potential is scanned in the positive direction, as evidenced by the emergence of a broad peak at about 515 mV when the concentration of $TCNQF_4$ is sufficiently high (Figure 3b,c). The oxidative stripping of the electrocrystallized $Cu^{I}TCNQF_4^{I-}{}_{(s)}$ from the electrode surface occurs as described in eq 5. If the concentrations of both $[Cu(MeCN)_4]^+$ and $TCNQF_4$ in the bulk solution are low, the electrocrystallization process is not favored. In contrast, the formation of a substantial quantity of $Cu^{I}TCNQF_4^{I-}{}_{(s)}$ follows the reduction of 2.0 mM $TCNQF_4$ in the presence of 100 mM $[Cu(MeCN)_4]^+$, at slow scan rates. Indeed, the reduction of $TCNQF_4$ to $TCNQF_4^{\bullet-}$ is irreversible at a scan rate of 10 mV s^{-1}. However, the i_p^{ox}/i_p^{red} ratio reverts to unity at faster scan rates ($\nu \geq 1$ V s^{-1}) (data not shown) as expected if the $TCNQF_4^{0/\bullet-}$ electrochemical process is followed by a kinetically controlled electrodeposition process.[34]

$$Cu^{I}TCNQF_{4(s)}^{I-} \rightarrow Cu^{+}{}_{(MeCN)} + TCNQF_{4(MeCN)} + e^{-} \quad (5)$$

(b). $Cu_2^{I}(TCNQF_4^{II-})(MeCN)_{2(s)}$. To electrocrystallize $Cu_2^{I}(TCNQF_4^{II-})(MeCN)_{2(s)}$, the voltammetry was extended to −600 mV. A requirement to achieve this outcome is that $Cu_2^{I}(TCNQF_4^{II-})(MeCN)_{2(s)}$ needs to be significantly less soluble than $Cu^{I}TCNQF_4^{I-}{}_{(s)}$ in a thermodynamic sense or that the rate of formation of $Cu^{I}TCNQF_4^{I-}{}_{(s)}$ is so slow that conditions can be chosen where $Cu_2^{I}(TCNQF_4^{II-})(MeCN)_{2(s)}$ can be formed but $Cu^{I}TCNQF_4^{I-}{}_{(s)}$ does not electrocrystallize prior to $TCNQF_4^{\bullet-}$ being reduced to $TCNQF_4^{2-}$. Voltammograms for 1.0 mM $TCNQF_4$ and 2.0 mM $[Cu(MeCN)_4]^+$ in acetonitrile (0.1 M Bu_4NPF_6) under conditions that meet the requirement of retention of the reversible $TCNQF_4^{0/\bullet-}$ solution phase process are shown in Figure 4a–c. As seen on examination of Figure 4a (black curve), on scanning in the negative direction at a low scan rate (20 mV s^{-1}), processes associated with the reduction of $TCNQF_4$ to $TCNQF_4^{\bullet-}$ (Red1) and then $TCNQF_4^{\bullet-}$ to $TCNQF_4^{2-}$ (Red2) are found. However, the process for oxidation of $TCNQF_4^{2-}$ to $TCNQF_4^{\bullet-}$, seen in the absence of $[Cu(MeCN)_4]^+$ (Figure 2a), is replaced by a sharp stripping peak at 280 mV (designated as Ox2). This outcome implies that under the chosen conditions $TCNQF_4^{2-}$ has rapidly combined with $Cu^{+}{}_{(MeCN)}$ to form solid $Cu_2^{I}(TCNQF_4^{II-})(MeCN)_{2(s)}$ (confirmed below), which adheres to the electrode surface. The $Cu_2^{I}(TCNQF_4^{II-})(MeCN)_{2(s)}$ is oxidized back to $TCNQF_4^{\bullet-}{}_{(MeCN)}$ and $Cu^{+}{}_{(MeCN)}$ (eq 6) at 280 mV (Ox2) as the potential is reversed in the positive direction. Interestingly, upon increasing the scan rate, a new oxidation process at ∼−130 mV (designated as Ox3) is detected and increases at the expense of the oxidation process Ox2 (Figure 4b). This behavior is consistent with the initial existence of a surface confined material prior to the formation of the final product $Cu_2^{I}(TCNQF_4^{II-})(MeCN)_{2(s)}$. Thus, the material formed or kinetically favored compound A (or phase A) is rapidly formed from reaction of $TCNQF_4^{2-}$ and $[Cu(MeCN)_4]^+$, which is then converted to the thermodynamically stable $Cu_2^{I}(TCNQF_4^{II-})(MeCN)_{2(s)}$ (compound B or phase B), as described in the reaction sequence given in eqs 7 and 8. This hypothesis is supported by simulations (see Section 3.3). $[Cu^{I}(MeCN)_2][Cu^{I}TCNQF_4^{II-}]$ or $[Cu^{I}(MeCN)_4][CuTCNQF_4^{II-}]$ would be likely candidates for intermediate A with a structure related to the $A[Cu^{I}TCNQF_4^{II-}]$ series reported in reference 24.

dx.doi.org/10.1021/ic500225v | Inorg. Chem. 2014, 53, 3230−3242

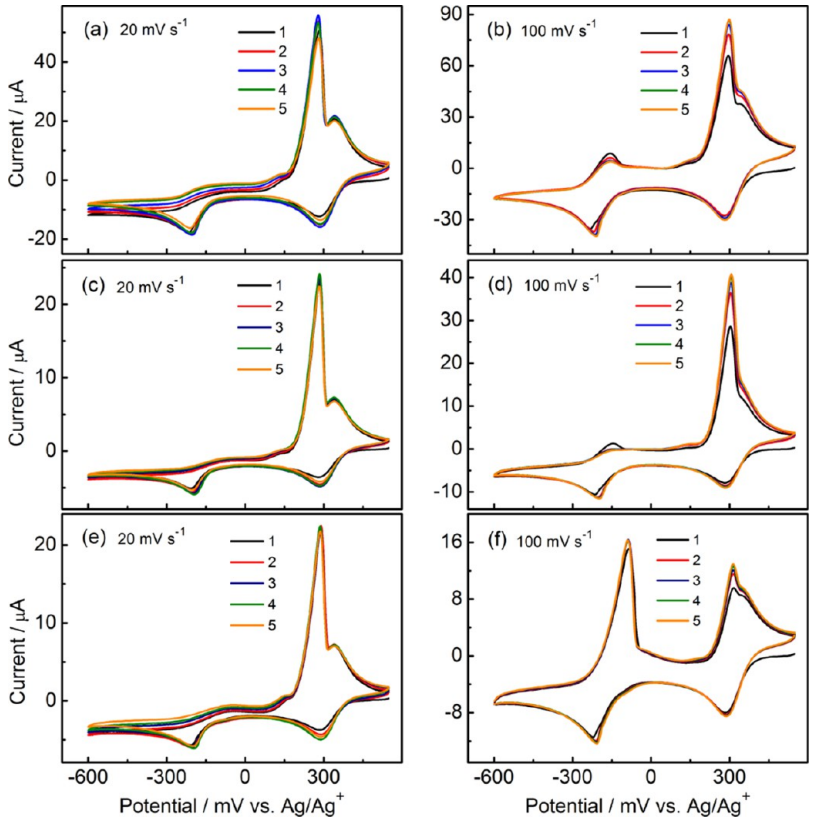

Figure 5. Cyclic voltammograms (first five cycles) obtained at (a,b) GC WE, (c,d) Pt, and (e,f) Au WE in an acetonitrile (0.1 M Bu_4NPF_6) solution containing 1.0 mM $TCNQF_4$ and 2.0 mM $[Cu(MeCN)_4]^+$ at scan rates of 20 and 100 mV s^{-1}.

$$Cu_2TCNQF_{4(s)} \rightarrow 2Cu^+_{(MeCN)} + TCNQF_{4(MeCN)} + e^- \quad (6)$$

$$2Cu^+_{(MeCN)} + TCNQF_{4(MeCN)^{2-}} \rightleftharpoons Cu_2(TCNQF_4)(MeCN)_{n(s,\text{compound A})} \quad (7)$$

$$Cu_2(TCNQF_4)(MeCN)_{n(s,\text{compound A})} \rightleftharpoons Cu_2^{I}(TCNQF_4^{II-})(MeCN)_{2(s,\text{compound B})} \quad (8)$$

Another series of experiments was conducted in which the potential was held at −400 mV for a period of time to electrocrystallize $Cu_2^{I}(TCNQF_4^{II-})(MeCN)_{2(s)}$ onto the GC electrode surface, followed by scanning the potential in the positive direction. Thus, when the potential was maintained at −400 mV for 1 s and then scanned in the positive direction (Figure 4c), the peak current associated with the oxidation of $Cu_2^{I}(TCNQF_4^{II-})(MeCN)_{2(s)}$ phase A (Ox3) increased significantly with scan rate, while that for the oxidation of $Cu_2^{I}(TCNQF_4^{II-})(MeCN)_{2(s)}$ phase B (Ox2) diminished and was no longer evident at fast scan rate. In addition, the peak asymmetry and other characteristics of the oxidation peaks Ox2 and Ox3 indicate that these processes are irreversible[34] as described in eq 6.

To confirm that the thus-far assumed stoichiometry for the reaction of Cu^+ and $TCNQF_4^{2-}$ is 2:1, cyclic voltammograms for a range of concentrations of $[Cu(MeCN)_4]^+$ and $TCNQF_4$ in acetonitrile (0.1 Bu_4NPF_6) solutions were recorded. When the concentration ratio $[Cu(MeCN)_4]^+/TCNQF_4 < 2:1$, in the reverse scan of the potential, the oxidation peak at −185 mV (Figure 4a - phase A, (A) on red curve) associated with the $TCNQF_4^{2-/\bullet-}$ diffusion-controlled process is observed, implying that $[Cu(MeCN)_4]^+$ concentration is not sufficient to react with all the $TCNQF_4^{2-}$, generated in the forward scan (Red2). In other words, to consume one $TCNQF_4^{2-}$ anion on the voltammetric time scale, 2 equiv of the $[Cu(MeCN)_4]^+$ cation is required.

3.1.3. Influence of Working Electrode Material on the Electrocrystallization of $Cu_2^{I}(TCNQF_4^{II-})(MeCN)_{2(s)}$. Cyclic voltammograms (first five cycles of the potential) for an acetonitrile (0.1 M Bu_4NPF_6) solution containing both 1.0 mM $TCNQF_4$ and 2.0 mM $[Cu(MeCN)_4]^+$ at scan rates of 20 and 100 mV s^{-1} are shown in Figure 5 as a function of electrode material. The behavior at the GC and Pt electrodes are similar. However, at the Au electrode, oxidation process Ox3 is more strongly favored at higher scan rates (cf. Figure 5d,f) than at the other surfaces examined. This implies that the precursor to $Cu_2^{I}(TCNQF_4^{II-})(MeCN)_{2(s)}$ formed on the Au electrode surface is relatively more stable than when adhered to the Pt or GC electrodes. However, the cyclic voltammetric behavior at all electrode surfaces is highly reproducible, implying that $TCNQF_4$ and $[Cu(MeCN)_4]^+$ are both regenerated at the end of each cycle.

3.1.4. Impact of $[Cu(MeCN)_4]^+$ Concentration and Scan Rate on the Electrocrystallization of $Cu_2^{I}(TCNQF_4^{II-})(MeCN)_{2(s)}$. Cyclic voltammetric studies on the reduction of 1.0 mM $TCNQF_4$ as a function of concentration of $[Cu(MeCN)_4]^+$ in acetonitrile (0.1 M Bu_4NPF_6) reveal that the peak potential for the $TCNQF_4^{0/\bullet-}$ reduction process is almost independent of $[Cu(MeCN)_4]^+$ concentration, as expected if the $TCNQF_4^{\bullet-}$ monoanion either does not react or interacts only weakly with the $[Cu(MeCN)_4]^+$ cation. In

dx.doi.org/10.1021/ic500225v | Inorg. Chem. 2014, 53, 3230−3242

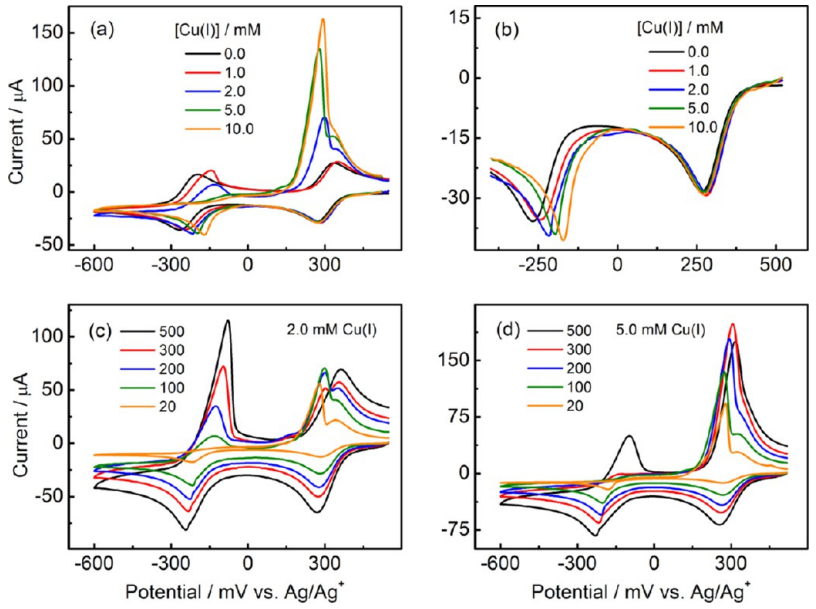

Figure 6. (a) Cyclic voltammograms for 1.0 mM $TCNQF_4$ in the presence of designated $[Cu(MeCN)_4]^+$ concentrations in acetonitrile (0.1 M Bu_4NPF_6) obtained with a 3.0 mm diameter GC electrode (v = 100 mV s^{-1}). (b) Same as for (a) but only reduction components are shown. (c,d) Same as for (a) but at designated scan rates and $[Cu(MeCN)_4]^+$ concentrations.

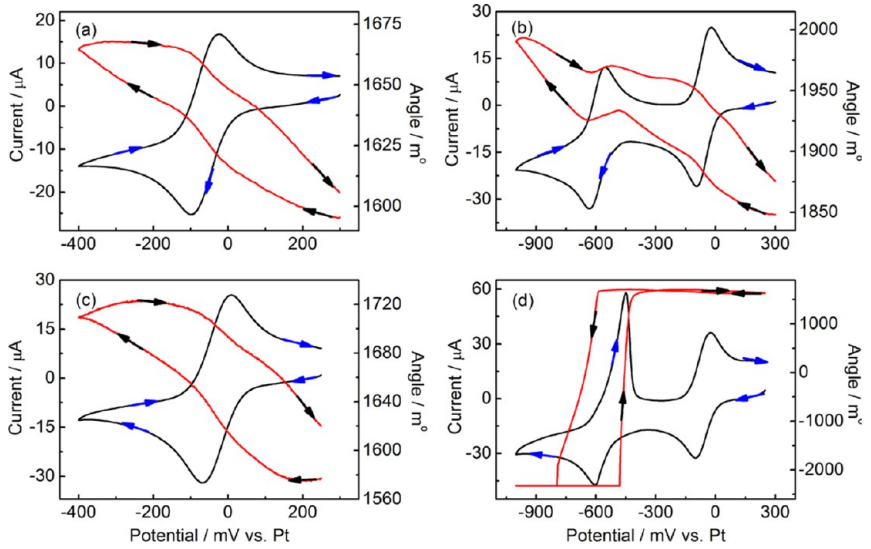

Figure 7. (black) In situ cyclic voltammetric and (red) SPR data obtained at a scan rate of 100 mV s^{-1} and as a function of switching potential when a gold electrode was in contact with acetonitrile (0.1 M Bu_4NPF_6) solutions containing 1.0 mM $TCNQF_4$ in (a,b) the absence and (c,d) the presence of 2.0 mM $[Cu(MeCN)_4]^+$.

contrast, the peak potential associated with the reduction of $TCNQF_4^{\bullet-}$ to $TCNQF_4^{2-}$ shifts by 97 mV to more positive values when the concentration of $[Cu(MeCN)_4]^+$ is increased from 0.0 mM to 10.0 mM (Figure 6a,b). Examination of Figure 6a also reveals that the peak current associated with the stripping of the intermediate decreases, while for $Cu_2^{I}(TCNQF_4^{II-})(MeCN)_{2(s)}$, an increase occurs as the concentration of $[Cu(MeCN)_4]^+$ is increased.

The results shown in Figure 6c,d are consistent with those in Figure 6a. Thus, for fixed scan rates from 20 to 500 mV s^{-1}, upon increasing the $[Cu(MeCN)_4]^+$ concentration from 2.0 to 5.0 mM, the peak currents associated with the oxidation of the intermediate and $Cu_2^{I}(TCNQF_4^{II-})(MeCN)_{2(s)}$ decrease and increase, respectively. The result of this series of experiments also is consistent with the hypothesis that a precusor to a final product $Cu_2^{I}(TCNQF_4^{II-})(MeCN)_{2(s)}$ is initially formed but is thermodynamically unstable. Analogous behavior to that shown at the GC electrode also was found at Pt and Au electrodes (data not shown), although there is a quantitative difference at the Au electrode as mentioned above.

3.2. In Situ Surface Plasmon Resonance and Electrochemical Quartz Crystal Microbalance Studies. The in situ mass changes taking place as a function of potential during the course of the cyclic voltammetric experiments at a gold electrode can be deduced by measurement of the concomitant change in the surface plasmon resonance (SPR), although the changes in the solution near the electrode surface also may affect the SPR intensity.[30,35,36] Figure 7 provides cyclic voltammetric–SPR responses at a gold electrode for 1.0 mM $TCNQF_4$ in acetonitrile (0.1 M Bu_4NPF_6) in the presence and

dx.doi.org/10.1021/ic500225v | Inorg. Chem. 2014, 53, 3230–3242

absence of 2.0 mM $[Cu(MeCN)_4]^+$. Upon reversing the potential scan direction between the $TCNQF_4^{0/\bullet-}$ and $TCNQF_4^{\bullet-/2-}$ reduction steps, the SPR signals obtained in the presence and absence of $[Cu(MeCN)_4]^+$ are almost indistinguishable (compare Figure 7a,c), implying that under these conditions, $Cu^ITCNQF_4^{I-}{}_{(s)}$ does not deposit onto the electrode surface. In contrast, when the potential is scanned to about −600 mV versus Pt wire to encompass the $TCNQF_4^{\bullet-/2-}$ reduction step, the SPR angle decreases severely to values that lie outside the detection capability of the instrument. Significantly, the SPR signal reverts to its initial value when the potential returns to the starting value (Figure 7d). These data confirm that mass increase occurs when the $TCNQF_4^{2-}$ dianion is generated and the electrocrystallization of the precursor to $Cu_2^I(TCNQF_4^{II-})(MeCN)_{2(s)}$ occurs on the gold electrode surface at negative potentials, and that mass is lost as the deposited solid is stripped from the surface. The data also confirm that conditions required to avoid the electrocrystallization of $Cu^ITCNQF_4^{I-}{}_{(s)}$ are available.

The EQCM technique also was applied to monitor the formation and stripping of $Cu_2^I(TCNQF_4^{II-})(MeCN)_{2(s)}$ from the surface of a gold electrode during the course of cyclic voltammetric experiments. Figure 8 shows the cyclic voltammogram (black curve) and mass change (red curve) derived from an acetonitrile (0.1 M Bu_4NPF_6) solution containing 1.0 mM $TCNQF_4$ in the presence of 2.0 mM $[Cu(MeCN)_4]^+$. The results are consistent with the SPR study. Thus, during the negative potential direction scan of the potential, no mass change on the electrode surface is observed until the reduction of $TCNQF_4^{\bullet-}$ to $TCNQF_4^{2-}$ occurs. This result confirms that under the chosen experimental conditions, the electrocrystallization of $Cu^ITCNQF_4^{I-}{}_{(s)}$ is avoided, while $Cu_2^I(TCNQF_4^{II-})(MeCN)_{2(s)}$ is electrocrystallized onto the electrode surface. When the potential was scanned back to the initial value, the mass on the electrode surface initially continued increasing and then decreased as the potential reached values where $Cu_2^I(TCNQF_4^{II-})(MeCN)_{2(s)}$ was stripped from the electrode. However, residual $Cu_2^I(TCNQF_4^{II-})(MeCN)_{2(s)}$ remained on the electrode surface as the mass change did not quite revert to zero.

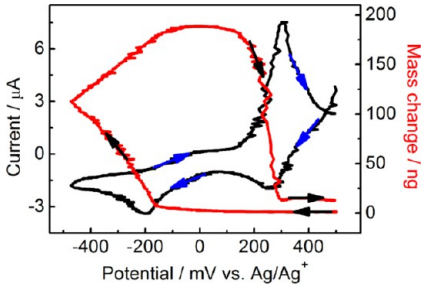

Figure 8. EQCM ((black) current, (red) mass change) data obtained with a 5.0 mm diameter Au electrode (ν = 20 mV s^{-1}) for an acetonitrile (0.1 M Bu_4NPF_6) solution containing 1.0 mM $TCNQF_4$ and 2.0 mM $[Cu(MeCN)_4]^+$.

3.3. Simulations of the Cyclic Voltammetry. Simulation software was used to mimic the voltammetry associated with the formation of electrocrystallized $Cu_2^I(TCNQF_4^{II-})(MeCN)_{2(s)}$ on an electrode surface that accompanies the reduction of $TCNQF_4$ to $TCNQF_4^{2-}$ in the presence of $[Cu(MeCN)_4]^+$ in acetonitrile (0.1 M Bu_4NPF_6). A comparison of simulated and experimental cyclic voltammograms is shown in Figure 9 over a range of scan rates. The hypothesis used in the simulation is that a kinetically favored phase A is formed initially from the reaction of $TCNQF_4^{2-}$ and $[Cu(MeCN)_4]^+$, which then rapidly converts to the thermodynamically stable $Cu_2^I(TCNQF_4^{II-})(MeCN)_{2(s)}$ as in eqs 7 and 8. Table 2 summarizes the parameters used to simulate the cyclic voltammograms that mimic the reduction of 1.0 mM $TCNQF_4$ in the presence of 2.0 mM $[Cu(MeCN)_4]^+$ in acetonitrile (0.1 M Bu_4NPF_6) at a 3.0 mm diameter GC electrode over the scan rate range of 20 to 500 mVs^{-1}. Clearly, the simulated and experimental cyclic voltammograms are in excellent agreement for the first and also subsequent cycles (data not shown) of the potential.

As shown above, under some conditions $TCNQF_4^{\bullet-}$ can react with $[Cu(MeCN)_4]^+$ to form $Cu^ITCNQF_4^{I-}{}_{(s)}$. However, the experimental conditions for simulations were chosen to minimize the contribution from this reaction (see Section 3.1.2a). This feature greatly simplifies the mechanism required for the simulations.

3.4. Characterization of the $Cu^ITCNQF_4^{I-}{}_{(s)}$ and $Cu_2^I(TCNQF_4^{II-})(MeCN)_{2(s)}$ Solids Prepared by Electrocrystallization and Electrochemically Directed Synthesis. EDXS was used to confirm the presence of the elements Cu, C, N, and F in the electrocrystallized $Cu^ITCNQF_4^{I-}{}_{(s)}$ and $Cu_2^I(TCNQF_4^{II-})(MeCN)_{2(s)}$ samples. However, to confirm the $TCNQF_4$ redox levels and other details, UV−vis,[2,37,38] FT-IR,[2,16−18,20,21] and Raman[2,18] spectroscopic and SEM imaging techniques were applied to electrocrystallized samples.

3.4.1. $Cu^ITCNQF_4^{I-}{}_{(s)}$ Prepared by Bulk Reductive Electrolysis of $TCNQF_4$. $Cu^ITCNQF_4^{I-}{}_{(s)}$ synthesized by the bulk reductive electrolysis of $TCNQF_4$ approach described in Section 2.2 was characterized spectroscopically and by other methods. As predicted from analysis of the cyclic voltammetry, $Cu^ITCNQF_4^{I-}{}_{(s)}$ has a finite level of solubility in acetonitrile. The UV−vis spectrum for $Cu^ITCNQF_4^{I-}{}_{(s)}$ dissolved in acetonitrile has three absorption bands with λ_{max} values at 411, 686, and 752 nm (see Figure S1a, Supporting Information), confirming that the $TCNQF_4^{\bullet-}$ radical anion is present after dissolution.[4,30,38] In the FT-IR spectrum for the solid (see Figure S1b, Supporting Information), the bands associated with the C≡N stretch are located at 2214 and 2187 cm^{-1}, which are similar to those at 2215 cm^{-1} and ∼2190 cm^{-1} reported for the compound in a previous study,[18] and typical for the monoanion[17] rather than the $TCNQF_4^{2-}$ dianion, where the IR bands are expected at ∼2167 and ∼2133 cm^{-1}.[38,39] The splitting of the C≡N stretch indicates that $TCNQF_4^{\bullet-}$ is coordinated to Cu^+ through the CN groups in $Cu^ITCNQF_4^{I-}{}_{(s)}$.[40] The Raman spectrum for $Cu^ITCNQF_4^{I-}{}_{(s)}$ (see Figure S1c, Supporting Information) exhibits bands at 2221 (C≡N stretch), 1641 (C═C ring stretch), 1439 (exocyclic C═C stretch), and 1273 cm^{-1} (mixing mode of C−F and ring C−C stretch). The Raman band at 1273 cm^{-1} is shifted to higher energy compared to that of 1193 cm^{-1} found for $TCNQF_4$, while the other three bands are located at lower energy, again as expected for the presence of the $TCNQF_4^{\bullet-}$ monoanion in $Cu^ITCNQF_4^{I-}{}_{(s)}$.[2,18]

To confirm that the molar ratio of $Cu^+/TCNQF_4^{\bullet-}$ in $Cu^ITCNQF_4^{I-}{}_{(s)}$ is 1:1, the solid was dissolved in acetonitrile with sonication for 5 min. 0.1 M Bu_4NPF_6 supporting electrolyte was then added into the saturated solution of $Cu^ITCNQF_4^{I-}$, and a steady-state voltammogram was recorded using a carbon-fiber microdisk electrode (Figure 10a). Clearly,

dx.doi.org/10.1021/ic500225v | Inorg. Chem. 2014, 53, 3230−3242

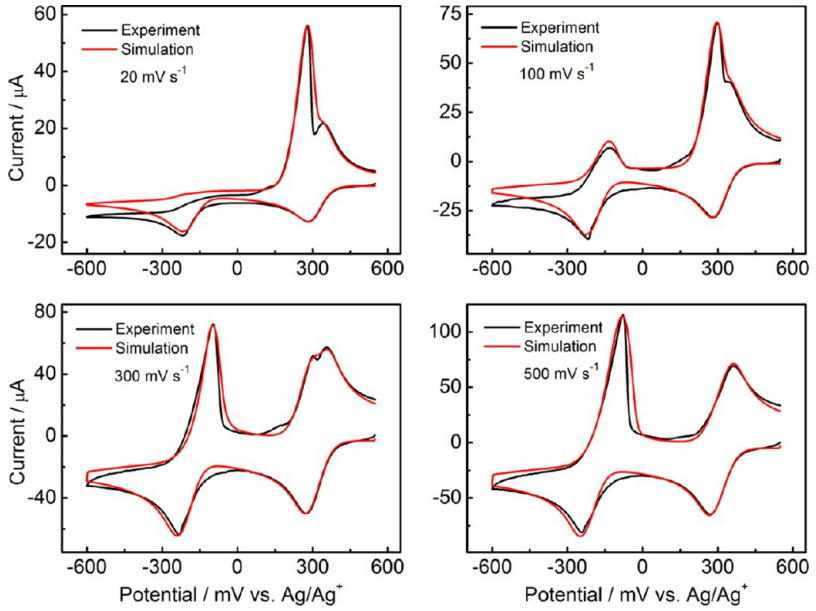

Figure 9. Comparison of (red) simulated and (black) experimental cyclic voltammograms obtained for 1.0 mM $TCNQF_4$ in the presence of 2.0 $[Cu(MeCN)_4]^+$ in acetonitrile (0.1 M Bu_4NPF_6) using a 3.0 mm diameter GC electrode at designated scan rates. Simulation parameters are provided in Table 2

Table 2. Parameters Used to Simulate Cyclic Voltammograms that Mimic the Reduction of 1.0 mM $TCNQF_4$ in the Presence of 2.0 mM $[Cu(MeCN)_4]^+$ in Acetonitrile (0.1 Bu_4NPF_6) when Using a 3.0 mm Diameter GC Electrode[a]

step	reaction	E^o (V)	k_s	K_{eq}	k_f[b]
1.	$T^c + e^- \rightarrow T^{\bullet-}$	0.315	0.1 cm s^{-1}[d]		
2.	$T^{\bullet-} + e^- \rightarrow T^{2-}$	−0.225	0.1 cm s^{-1}[d]		
3.	$T^{2-} + Cu^+ \rightarrow CuT^-$			1×10^8	1×10^5[d]
4.	$CuT^- + Cu^+ \rightarrow Cu_2TA$			1×10^6	1×10^{10}
5.	$Cu_2TA \rightarrow Cu_2TB$[f]			1×10^{15}	1[d]
6.	$Cu_2TA \rightarrow Cu_2TA^*$			1×10^{15}	1×10^{10}
7.	$Cu_2TB \rightarrow Cu_2TB^*$			1×10^{20}	1×10^{10}
8.	$Cu_2TA \rightarrow Cu_2TA^+ + e^-$	−1.30	0.0 cm s^{-1}[g]		
9.	$Cu_2TB \rightarrow Cu_2TB^+ + e^-$	−1.16	0.0 cm s^{-1}[g]		
10.	$Cu_2TA^* \rightarrow Cu_2TA^{*+} + e^-$	−0.117[h]	50 s^{-1}[d]		
11.	$Cu_2TB^* \rightarrow Cu_2TB^{*+} + e^-$	0.319[h]	50 s^{-1}[d]		
12.	$Cu_2TA^{*+} \rightarrow Cu_2TA^+$			1×10^5	1×10^2[d]
13.	$Cu_2TB^{*+} \rightarrow Cu_2TB^+$			1×10^5	1×10^2
14.[i]	$Cu_2TA^+ \rightarrow T^{\bullet-} + Cu_2^{2+}$			1×10^{15}	1×10^6
15.[i]	$Cu_2TB^+ \rightarrow T^{\bullet-} + Cu_2^{2+}$			232.3[h]	1×10^6
16.[i]	$Cu_2^{2+} \rightarrow Cu^+ + Cu^+$			6.8×10^{-48}[h]	1×10^{12}

[a]Other parameters used in the simulation are: $\alpha = 0.50$, $T = 295$ K, area of electrode = 0.074 cm^2; uncompensated resistance $R_u = 200\ \Omega$; double layer capacitance $C_{dl} = 1 \times 10^{-5}$ F; diffusion coefficients: $TCNQF_4 = 2.0 \times 10^{-5}$, $TCNQF_4^{\bullet-} = 1.9 \times 10^{-5}$, $TCNQF_4^{2-} = 1.5 \times 10^{-5}$;[22] $Cu^+ = 2.3 \times 10^{-5}$ cm^2 s^{-1} (determined from peak currents derived from cyclic voltammograms for reduction of 2.0 mM $Cu(MeCN)_4^+$ in acetonitrile (0.1 M Bu_4NPF_6) obtained with a 3.0 mm diameter GC electrode at different scan rates using the Randles−Sevcik relationship $i_p = 0.4463nFAC(nF\nu D/RT)^{1/2}$; this value is consistent with a previous report[47] for diffusion coefficient of $[Cu(MeCN)_4]^+$ in acetonitrile being 2.2×10^{-5} cm^2 s^{-1} at 38 °C), and 1.0×10^{-5} cm^2 s^{-1} for all other species (note that varying the diffusion coefficient of intermediate specices almost does not affect the simulated cyclic voltammetric behavior), the maximum surface coverage ≈ 10^{-9} moles cm^{-2}, self-interaction parameter $a^* = 0$. [b]k_f has unit of M^{-1} s^{-1} for steps 3 and 4 (second-order reactions) and s^{-1} for other steps (first-order reactions). [c]T = $TCNQF_4$. [d]In some cases, the value of this parameter may be slightly varied from those stated to provide enhanced agreement between simulated and experimental cyclic voltammograms; in other cases, simulation can be insensitive to particular value; e.g., in steps 1 and 2, any k_s values of >0.1 cm s^{-1} allow excellent agreement between simulation and experiment to be obtained, so that the value of 0.1 cm s^{-1} represents a lower limit. [e]Cu_2TA = form A of $Cu_2TCNQF_{4(s)}$. [f]Cu_2TB = form B of $Cu_2TCNQF_{4(s)}$. [g]Oxidation of dissovled form A and B in solution is switched off in the simulation; i.e., form A and $Cu_2^I(TCNQF_4^{II-})(MeCN)_{2(s)}$ (form B) are strongly adhered to the electrode surface. However, the E^0 values for these processes have to be included to generate those (created automatically by the software) needed for steps 10 and 11. [h]Values of these parameters are automatically computed by the DigiElch software from other input parameters (thermodynamically related data). [i]$Cu_2^I(TCNQF_4^{II-})(MeCN)_2$ might fully dissociate into $TCNQF_4^{\bullet-}$ and $2Cu^+$ in a single step, but the simulation software does not allow for this possibility.

the limiting currents associated with the reduction of $TCNQF_4^{\bullet-}$ and $[Cu(MeCN)_4]^+$ are consistent with the ratio

dx.doi.org/10.1021/ic500225v | Inorg. Chem. 2014, 53, 3230−3242

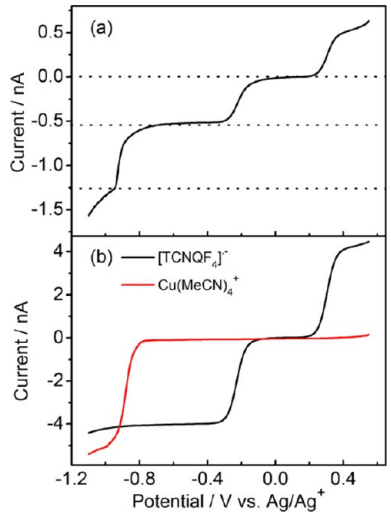

Figure 10. Near steady-state voltammograms obtained with a 11 μm diameter carbon-fiber microelectrode (v = 20 mV s^{-1}) for acetonitrile (0.1 Bu_4NPF_6) solutions containing (a) saturated $Cu^{I}TCNQF_4^{I-}$ and (b) 1.0 mM $TCNQF_4^{\bullet-}$ and 1.0 mM $[Cu(MeCN)_4]^+$.

of $Cu^+/TCNQF_4^{\bullet-}$ of 1:1 as the relative limiting currents are the same as those found for individual prepared solutions of either 1.0 mM $TCNQF_4^{\bullet-}$ or $[Cu(MeCN)_4]^+$ (Figure 10b).

3.4.2. Electrocrystallized $Cu^{I}TCNQF_4^{I-}{}_{(s)}$. $Cu^{I}TCNQF_4^{I-}{}_{(s)}$ was electrocrystallized onto the surface of an ITO electrode by reduction of 2.0 mM $TCNQF_4$ in acetonitrile (0.1 M Bu_4NPF_6) containing 10.0 mM $[Cu(MeCN)_4]^+$. In this case, the potential at the ITO electrode was held at 100 mV for 15 min. The electrocrystallized solid was rinsed with ethanol, dried under a stream of N_2 gas for 10 min, and finally placed in vacuum overnight before being characterized. UV–vis, FT-IR, and Raman spectra for the electrocrystallized $Cu^{I}TCNQF_4^{I-}{}_{(s)}$ are indistinguishable from those reported above from bulk electrochemical synthesis of $Cu^{I}TCNQF_4^{I-}{}_{(s)}$. The morphology of $Cu^{I}TCNQF_4^{I-}{}_{(s)}$ electrocrystallized onto the ITO electrode surface was probed via SEM. A film of closely packed microcrystals of micrometer size was formed (Figure 11).

3.4.3. Characterization of $Cu_2^{I}(TCNQF_4^{II-})(MeCN)_{2(s)}$. To establish that solvent is present in $Cu_2^{I}(TCNQF_4^{II-})(MeCN)_{2(s)}$ prepared by directed bulk electrolysis as described in Section 2.1, TGA experiments were undertaken over the temperature range of 25 to 350 °C. Results show that at about 140 °C, the compound loses 17.0 ± 1% of its mass (see Figure S2, Supporting Information). This is consistent with the empirical formula being $Cu_2^{I}(TCNQF_4^{II-})(MeCN)_2$ with the calculated mass due to CH_3CN being 16.92%. The CH_3CN mass loss occurs at such high temperature relative to its pure solvent boiling point of 82 °C so that MeCN is likely to be coordinated to the copper ions.

The FT-IR spectrum of $Cu_2^{I}(TCNQF_4^{II-})(MeCN)_{2(s)}$ is provided in Figure S3a of the Supporting Information. IR bands associated with the C≡N stretch are located at 2204, 2162, and 2135 cm^{-1}. The bands at 2162 and 2135 cm^{-1} are in accord with the presence of the $TCNQF_4^{2-}$ dianion as reported in studies on $[Fe(C_5Me_5)_2]_2(TCNQF_4)$ and $[Co(C_5Me_5)_2]_2(TCNQF_4)$ (~2167 and 2133 cm^{-1}),[38] $[Ni(C_5Me_5)_2]_2(TCNQF_4)$ (2167 and 2131 cm^{-1}),[39] and a Mn^{II}-$TCNQF_4^{2-}$-based compound (2161 cm^{-1}).[21] The IR band at 2204 cm^{-1} is attributed to the presence of photogenerated $TCNQF_4^{\bullet-}$,[17,19,21] resulting from photoinduced transformation of $TCNQF_4^{2-}$ to $TCNQF_4^{\bullet-}$ (via the internal redox reaction summarized in eq 9). Phototransformation is facilitated by irradiation from the laser beam used to record the IR spectra, as reported in studies on $Cu_2TCNQF_{4(s)}$[16] and also for $Ag_2TCNQF_{4(s)}$.[16,30] However, the rate of the transformation of $TCNQF_4^{2-}$ in $Cu_2^{I}(TCNQF_4^{II-})(MeCN)_{2(s)}$ to $TCNQF_4^{\bullet-}$ upon irradiation with white light is very slow compared to that found with $Ag_2TCNQF_{4(s)}$.[30] Slow photochemical conversion also has been confirmed by UV–vis spectroscopy. Thus, after being synthesized as in Section 2.2, $Cu_2^{I}(TCNQF_4^{II-})(MeCN)_2$ solid was dissolved in acetonitrile and centrifuged to provide a saturated solution. Although the solubility of $Cu_2^{I}(TCNQF_4^{II-})(MeCN)_{2(s)}$ is very low, the concentration of $TCNQF_4^{2-}$ (λ_{max} = 333 nm)[23] is still sufficient for detection by UV–vis spectroscopy, along with a very small quantity of $TCNQF_4^{\bullet-}$ (λ_{max} = 411 nm).[23,30] However, on leaving the

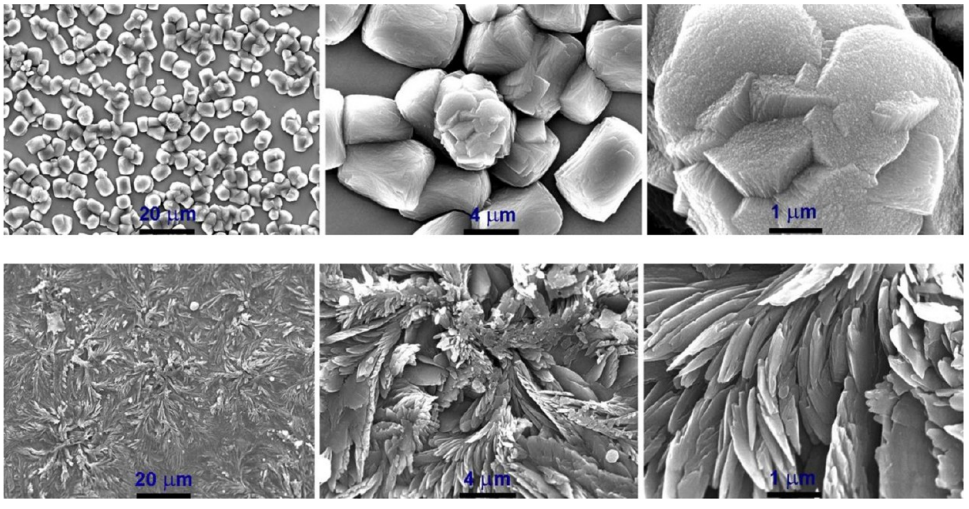

Figure 11. SEM images at increasing magnification (left to right): (top): for $Cu^{I}TCNQF_4^{I-}$ electrocrystallized onto an ITO electrode surface from an acetonitrile (0.1 M Bu_4NPF_6) solution containing 2.0 mM $TCNQF_4$ and 10.0 mM $[Cu(MeCN)_4]^+$. Reductive electrolysis of $TCNQF_4$ to $TCNQF_4^{\bullet-}$ was for 15 min at 100 mV; (bottom): for $Cu_2^{I}(TCNQF_4^{II-})(MeCN)_{2(s)}$ electrocrystallized onto an ITO electrode surface by reductive electrolysis of 1.0 mM $TCNQF_4$ at −500 mV for 15 min in an acetonitrile (0.1 M Bu_4NPF_6) solution containing 2.0 mM $[Cu(MeCN)_4]^+$.

dx.doi.org/10.1021/ic500225v | Inorg. Chem. 2014, 53, 3230–3242

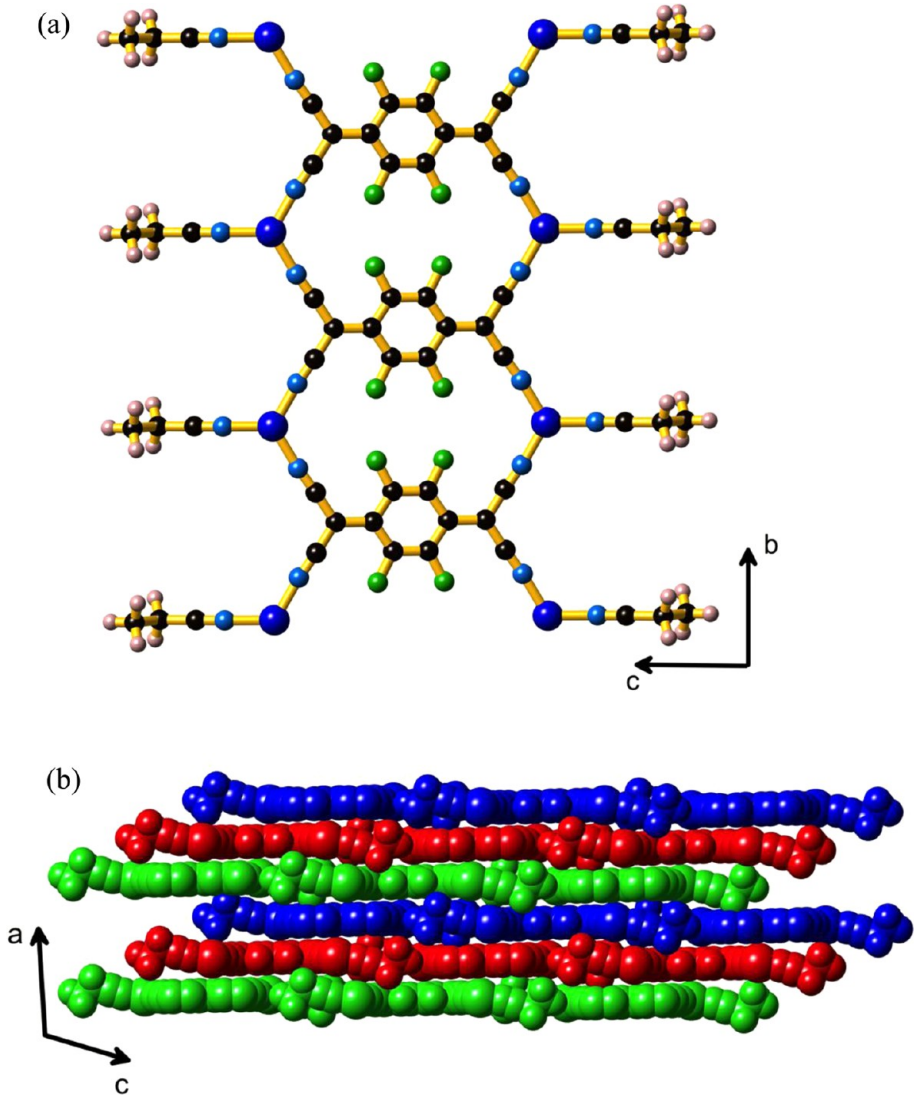

Figure 12. The single-crystal X-ray structure of $Cu_2(TCNQF_4)(EtCN)_2$ showing (a) a ball and stick representation of part of a single infinite strip; color code: Cu blue, F green, N light blue, C black, H pink, and (b) a space-filling representation, viewed along the direction of the strips, indicating the ABCABC stacking arrangement of the sheets; each sheet indicated is three strips wide.

sample for several days, even under vacuum, the relative quantity of $TCNQF_4^{\bullet-}$ in the solid increased (data not shown).

$$(m+n)(Cu^{I})_2(TCNQF_4^{II-})_{(s)} \xrightarrow{h\nu} mCu^{0}_{(s)} + mCu^{I}TCNQF_{4(s)}^{I-} + n(Cu^{I})_2(TCNQF_4^{II-})_{(s)} \quad (9)$$

An optically induced transformation also occurs with $Cu^{I}TCNQ^{I-}$.[41−43] Thus, $Cu^{I}TCNQ^{I-}$ undergoes the transformation given in eq 10 when irradiated with visible light,[41] or exposed to green light used to record Raman spectra when above a threshold power value,[42] or a laser diode beam intensity.[43] However, the transformation of $Cu_2^{I}(TCNQF_4^{II-})(MeCN)_2$ is thermodynamically more favored as E_m for the $TCNQF_4^{\bullet-/2-}$ process is −170 mV more negative than that for the $TCNQ^{0/\bullet-}$ one,[23] that is, $TCNQF_4^{2-}$ is a stronger reductant than $TCNQ^{\bullet-}$.

$$(m+n)Cu^{+}TCNQ^{\bullet-}_{(s)} \xrightarrow{h\nu} mCu^{0}_{(s)} + mTCNQ_{(s)} + nCu^{+}TCNQ^{\bullet-}_{(s)} \quad (10)$$

The IR bands at 1475 and 1489 cm^{-1} are also characteristic of $TCNQF_4^{2-}$, as found at 1477 and 1495 cm^{-1} in Ag_2TCNQF_4.[16] The analogous bands[16] are located at 1494 and 1528 cm^{-1} in $Cu^{I}TCNQF_4^{I-}$ (see Figure S1b, Supporting Information), so in $Cu_2^{I}(TCNQF_4^{II-})(MeCN)_{2(s)}$, they are shifted by 19 and 39 cm^{-1}, respectively, to lower energy. A similar shift also is found in comparing IR bands for $AgTCNQF_4$ and Ag_2TCNQF_4.[16] Although the TGA experiment indicates the presence of two moles of coordinated CH_3CN, as expected for a $[Cu(CH_3CN)_2]^+$ cation, no IR bands at around 2300 cm^{-1} for the C≡N stretch in coordinated CH_3CN (2290 cm^{-1} in $Cr(TCNQ)_2(CH_3CN)_2$[44] or at 2274, 2302, and 2310 cm^{-1} in $[Cu(CH_3CN)_4]PF_6$ were detected. Also no CH_3CN IR band, analogous to that was found for the coordination polymer containing the $[Cu^{I}(CH_3CN)_2]^+$ cation by Perruchas et al.,[45] was detected.

The Raman vibration region for the C≡N stretch in the $Cu_2^{I}(TCNQF_4^{II-})(MeCN)_{2(s)}$ consists of three bands located at 2218, 2170, and 2141 cm^{-1} (See Figure S4a, Supporting Information). The vibration mode at 2218 cm^{-1} is consistent with the presence of $TCNQF_4^{\bullet-}$,[2,18,30] again attributed to

dx.doi.org/10.1021/ic500225v | Inorg. Chem. 2014, 53, 3230−3242

photoinduced transformation of $TCNQF_4^{2-}$ to $TCNQF_4^{\bullet-}$ during recording of the Raman spectrum, while the two bands located at lower energy are consistent with $TCNQF_4^{2-}$-based material. The Raman bands at 1655, 1435, and 1246 cm^{-1} are attributed to C=C ring, exocyclic stretch, and mixed C−F and ring C−C stretches, respectively, in $TCNQF_4^{2-}$, while other bands at 1643, 1443, and 1273 cm^{-1} are in accord with these stretches in $TCNQF_4^{\bullet-}$, as discussed in Section 3.4.1.

$Cu_2^{I}(TCNQF_4^{II-})(MeCN)_{2(s)}$ electrocrystallized onto an ITO electrode surface from 1.0 mM $TCNQF_4$ and 2.0 mM $[Cu(MeCN)_4]^+$ in acetonitrile (0.1 M Bu_4NPF_6) following reduction of $TCNQF_4$ to $TCNQF_4^{2-}$ at a constant potential of −500 mV for 15 min was rinsed with 3 × 3 mL of acetonitrile, dried under a stream of N_2 gas for 10 min, and then was put under vacuum overnight before being spectroscopically characterized. FT-IR, Raman, and UV−vis spectra for this electrocrystallized $Cu_2^{I}(TCNQF_4^{II-})(MeCN)_{2(s)}$ sample are identical (within experimental error) with the solid synthesized by bulk electrolysis (see Figures S3 and S4, Supporting Information, UV−vis spectra not shown). Spectroscopic data imply that Cu^+-$TCNQF_4^{2-}$-based compounds isolated by the two methods have the same structure and are both prone to optically induced transformation to $Cu^{I}TCNQF_4^{I-}$ and Cu metal. SEM images reveal that the rod-like morphology of the electrocrystallized $Cu_2^{I}(TCNQF_4^{II-})(MeCN)_{2(s)}$ differs from that of electrocrystallized $Cu^{I}TCNQF_4^{I-}$, which is closely packed cubic particles (Figure 11).

Elemental analysis data for the $Cu_2^{I}(TCNQF_4^{II-})(MeCN)_{2(s)}$ synthesized by the bulk electrolysis method from acetonitrile solutions of $[Cu(MeCN)_4]^+$ and $TCNQF_4^{2-}$ are: found %C = 39.50; %H = 1.26; %N = 17.48, (calculated: %C = 39.59, %H = 1.25, %N = 17.32), which is consistent with the formulation $Cu_2^{I}(TCNQF_4^{II-})(MeCN)_2$.

$Cu_2^{I}(TCNQF_4^{II-})(MeCN)_2$ was also obtained by chemical synthesis of $[Cu(CH_3CN)_4]^+$ and H_2TCNQF_4 in acetonitrile in the presence of a weak base, using the procedure described in Section 2.2 for the preparation of $A[Cu^{I}(TCNQF_4)^{II-}]$. Repeated attempts to obtain single crystals of $Cu_2^{I}(TCNQF_4^{II-})(MeCN)_2$ of a quality appropriate for single-crystal diffraction studies were unsuccessful, although weakly diffracting microcrystals as deduced from XRD powder patterns were found for chemically and electrochemically synthesized samples (see Figure S5, Supporting Information). However when propionitrile was used instead of acetonitrile, suitable crystals of composition, $Cu_2(TCNQF_4)(EtCN)_2$, were obtained. The crystal structure determination of $Cu_2(TCNQF_4)(EtCN)_2$ indicates that $TCNQF_4^{2-}$ units are located on sites of 2/*m* symmetry. Each of these dianions is bound to four Cu(I) centers that are located at the corners of rectangles of dimensions 10.64 × 7.53 Å (Figure 12a). Each Cu(I) center is coordinated to two $TCNQF_4^{2-}$ units and a propionitrile ligand leading to a trigonal coordination environment around the metal center with N−Cu−N angles in the range of 119.2−120.2°; Cu−N distances are all similar [Cu−N($TCNQF_4$) 1.911(2) Å, Cu−N(EtCN) 1.931(3) Å]. The edge-sharing along the long edge of these rectangular units leads to the formation of infinite strips that extend along the *b*-axis.

Interdigitation of propionitrile ligands belonging to parallel coplanar strips leads to the generation of a two-dimensional sheet as indicated in Figure S6 of the Supporting Information. These sheets stack on top of each other in an ABCABC sequence as indicated in Figure 12b. The mean separation between the sheets is approximately 3.36 Å, with some contacts between pairs of carbon atoms being less than 3.30 Å. Specstroscopic data for $Cu_2(TCNQF_4)(EtCN)_2$ are very similar to that of $Cu_2^{I}(TCNQF_4^{II-})(MeCN)_2$ (see Figures S3 and S4, Supporting Information).

3.5. Solubility of $Cu^{I}TCNQF_4^{I-}{}_{(s)}$ and $Cu_2^{I}(TCNQF_4^{II-})(MeCN)_{2(s)}$ in Acetonitrile. The solubility of $Cu^{I}TCNQF_4^{I-}{}_{(s)}$ in acetonitrile in the presence and absence of 0.1 M Bu_4NPF_6 supporting electrolyte was determined. Thus, 2.0 mL of acetonitrile containing 0.1 M Bu_4NPF_6 supporting electrolyte or neat acetonitrile were used to dissolve $Cu^{I}TCNQF_4^{I-}{}_{(s)}$ synthesized as described in Section 2.2. The mixtures were then sonicated for 5 min to achieve equilibrium between the solid and solution phases. The concentrations of $TCNQF_4^{\bullet-}$ in the saturated solutions were determined by UV−vis spectroscopy, using the absorption band with λ_{max} at 411 nm and reference to a calibration curve. In this manner, the concentration of $TCNQF_4^{\bullet-}$ was determined to be $(1.95 \pm 0.06) \times 10^{-4}$ M and $(1.14 \pm 0.03) \times 10^{-4}$ M in the presence and absence of 0.1 M Bu_4NPF_6, respectively. Consequently, the solubility products of the $Cu^{I}TCNQF_4^{I-}{}_{(s)}$ in acetonitrile containing 0.1 M Bu_4NPF_6 supporting electrolyte and in neat solvent are $(3.81 \pm 0.25) \times 10^{-8}$ M^2 and $(1.30 \pm 0.07) \times 10^{-8}$ M^2, respectively.

The solubility of $Cu_2^{I}(TCNQF_4^{II-})(MeCN)_{2(s)}$ in acetonitrile in the presence and absence of 0.1 M Bu_4NPF_6 was determined in a similar manner to that for the $Cu^{I}TCNQF_4^{I-}{}_{(s)}$. However, to achieve a saturated $Cu_2^{I}(TCNQF_4^{II-})(MeCN)_2$ solution, instead of sonication, a mixture of $Cu_2^{I}(TCNQF_4^{II-})(MeCN)_2$ solid and acetonitrile was purged with N_2 gas for 10 min to achieve equilibration ($TCNQF_4^{2-}$ slowly decomposes in the presence of air). The concentration of $TCNQF_4^{2-}$ in each of the $Cu_2^{I}(TCNQF_4^{II-})(MeCN)_2$ saturated solutions after filtration was determined by UV−vis spectroscopy, using the band with λ_{max} at 333 nm and a calibration curve, to be $1.59 \pm 0.06 \times 10^{-5}$ M and $(7.29 \pm 0.46) \times 10^{-6}$ M in 0.1 M Bu_4NPF_6 containing and neat acetonitrile, respectively, leading to $Cu_2^{I}(TCNQF_4^{II-})(MeCN)_{2(s)}$ solubility products of $(1.61 \pm 0.17) \times 10^{-14}$ M^3 and $(1.55 \pm 0.20) \times 10^{-15}$ M^3, respectively. The solubility of $Cu^{I}TCNQF_4^{I-}{}_{(s)}$ and $Cu_2^{I}(TCNQF_4^{II-})(MeCN)_{2(s)}$ in the presence of 0.1 M Bu_4NPF_6 supporting electrolyte is higher than that in neat acetonitrile. The enhanced solubility, also found for $AgTCNQ_{(s)}$ and $CuTCNQ_{(s)}$, is attributed to the ion paring[30,46] of Cu^+, $TCNQF_4^{\bullet-}$, and $TCNQF_4^{2-}$ with counterions provided by the Bu_4NPF_6 supporting electrolyte.

4. CONCLUSIONS

Electrochemically directed synthesis of $Cu^{I}TCNQF_4^{I-}{}_{(s)}$ and $Cu_2^{I}(TCNQF_4^{II-})(MeCN)_{2(s)}$ has been achieved via reduction of $TCNQF_4$ to $TCNQF_4^{\bullet-}$ and $TCNQF_4^{2-}$, respectively, in acetonitrile (0.1 M Bu_4NPF_6), followed by reaction with $[Cu(MeCN)_4]^+$. The solubility of the $Cu^{I}TCNQF_4^{I-}{}_{(s)}$ and $Cu_2^{I}(TCNQF_4^{II-})(MeCN)_{2(s)}$ in acetonitrile in the presence and absence of 0.1 M Bu_4NPF_6 supporting electrolyte has been determined to be $(1.95 \pm 0.06) \times 10^{-4}$ M and $(1.14 \pm 0.03) \times 10^{-4}$ M (for $Cu^{I}TCNQF_4^{I-}{}_{(s)}$), and $(1.59 \pm 0.06) \times 10^{-5}$ M and $(7.29 \pm 0.46) \times 10^{-6}$ M (for $Cu_2^{I}(TCNQF_4^{II-})(MeCN)_{2(s)}$), respectively. Thus, $Cu_2^{I}(TCNQF_4^{II-})(MeCN)_{2(s)}$ is more than 10-fold less soluble than $Cu^{I}TCNQF_4^{I-}{}_{(s)}$. This allows $Cu_2^{I}(TCNQF_4^{II-})(MeCN)_2$ to be electrocrystallized from low concentrations of $TCNQF_4$ and $[Cu(MeCN)_4]^+$, while $Cu^{I}TCNQF_4^{I-}$ may be electrocrystal-

dx.doi.org/10.1021/ic500225v | Inorg. Chem. 2014, 53, 3230−3242

lized from higher concentration environments. Inspection of Figure 12b reveals that in the structure of $[Cu_2(TCNQF_4)(EtCN)_2]$, parallel strips, forming sheets, stack directly on top of each other. If $Cu_2^{I}(TCNQF_4^{II-})(MeCN)_2$ adopts a similar structure in which extensive face-to-face contact is made between parallel sheets, then a relatively high degree of insolubility may be expected. UV−vis, IR, and Raman spectra confirm the presence of either $TCNQF_4^{\bullet-}$ or $TCNQF_4^{2-}$ as appropriate in all materials synthesized by electrochemical bulk electrolysis or electrocrystallization. $Cu_2^{I}(TCNQF_4^{II-})(MeCN)_{2(s)}$ undergoes slow photoinduced transformation to $Cu^{I}TCNQF_4^{I-}{}_{(s)}$ and metallic Cu via an internal redox reaction. Electrocrystallized $Cu^{I}TCNQF_4^{I-}{}_{(s)}$ produced cubic particles (~3 μm), while $Cu_2^{I}(TCNQF_4^{II-})(MeCN)_{2(s)}$ formed with a rod-shaped morphology. A simulation that mimics the electrocrystallization of $Cu_2^{I}(TCNQF_4^{II-})(MeCN)_{2(s)}$ from the reduction of $TCNQF_4$ to $TCNQF_4^{2-}$ in the presence of $[Cu(MeCN)_4]^+$ in acetonitrile (0.1 M Bu_4NPF_6) is proposed and describes most of the features present in experimental cyclic voltammograms over a range of scan rates. Electrocrystallization experiments imply that a different phase or compound with different MeCN formulation is initially formed in a thermodynamically unstable form, which rapidly converts to $Cu_2^{I}(TCNQF_4^{II-})(MeCN)_2$. While a single-crystal structure determination of $Cu_2^{I}(TCNQF_4^{II-})(MeCN)_2$ was not possible, the structure of $Cu_2(TCNQF_4)(EtCN)_2$ was successfully determined. It is reasonable, given the similarity in composition and spectroscopy to expect that $Cu_2^{I}(TCNQF_4^{II-})(MeCN)_2$ adopts a very similar strip-like structure to the propionitrile analogue. TGA, elemental analysis, and FT-IR are all consistent with the formulation $Cu_2^{I}(TCNQF_4^{II-})(MeCN)_2$. Importantly, electrochemical synthesis of $TCNQF_4^{2-}$ complexes is facilitated relative to $TCNQ^{2-}$-based materials due to their much-reduced level of reactivity with oxygen. It is now clear that Cu^{I}-$TCNQF_4^{I-}$ and Cu^{I}-$TCNQF_4^{II-}$ derivatives are accessible in chemically pure form. The relationship to Cu-TCNQ-doped nanocrystal of Cu/TCNQ ratio of 1.3:1 containing both the $TCNQ^{\bullet-}$ anion radical and $TCNQ^{2-}$ dianion is therefore most intriguing.

■ ASSOCIATED CONTENT

Ⓢ Supporting Information

UV, IR, and Raman spectra for $TCNQF_4$, $Cu^{I}TCNQF_4^{I-}$, and $Cu_2^{I}(TCNQF_4^{II-})(MeCN)_2$, TGA and XRD powder pattern data for $Cu_2^{I}(TCNQF_4^{II-})(MeCN)_2$, X-ray crystallographic information file (cif) and representation of the structure of $Cu_2^{I}(TCNQF_4^{II-})(EtCN)_2$. This material is available free of charge via the Internet at http://pubs.acs.org

■ AUTHOR INFORMATION

Corresponding Authors

*E-mail: Alan.Bond@monash.edu (A.M.B.).
*E-mail: Lisa.Martin@monash.edu (L.L.M.).

Present Addresses

[¶]Le Quy Don High School for the Gifted, Danang City, Vietnam.
[§]King Saud University, College of Science, Department of Chemistry, P.O. Box 2455, Riyadh 11451, Saudi Arabia.

Notes

The authors declare no competing financial interest.

■ ACKNOWLEDGMENTS

Financial support from the Australian Research Council to A.M.B., L.L.M., B.F.A., and R.R., a graduate scholarship from Danang City in Vietnam and a top-up stipend award from Monash University Faculty of Science Dean's International Postgraduate Research Scholarship to T.H.L. as well as a Monash Graduate Scholarship and Monash International Postgraduate Research Scholarship to N.T.V. are greatly appreciated. We gratefully acknowledge Dr. Stephen Feldberg for discussions on the digital simulations, the Monash Electron Microscopy Center for obtaining the SEM images, and Finlay Shanks for technical assistance with the TGA experiments.

■ REFERENCES

(1) Zhao, H.; Heintz, R. A.; Ouyang, X.; Dunbar, K. R.; Campana, C. F.; Rogers, R. D. *Chem. Mater.* **1999**, *11*, 736−746.
(2) Xiao, K.; Rondinone, A. J.; Puretzky, A. A.; Ivanov, I. N.; Retterer, S. T.; Geohegan, D. B. *Chem. Mater.* **2009**, *21*, 4275−4281.
(3) Lu, J.; Loh, K. P. *Chem. Phys. Lett.* **2009**, *468*, 28−31.
(4) Maity, A. N.; Sarkar, B.; Niemeyer, M.; Sieger, M.; Duboc, C.; Zalis, S.; Kaim, W. *Dalton Trans.* **2008**, 5749−5753.
(5) Azcondo, M. T.; Ballester, L.; Golhen, S.; Gutierrez, A.; Ouahab, L.; Yartsev, S.; Delhaes, P. *J. Mater. Chem.* **1999**, *9*, 1237−1244.
(6) Ran, C. B.; Peng, H. L.; Zhou, W.; Yu, X. C.; Liu, Z. F. *J. Phys. Chem. B* **2005**, *109*, 22486−22490.
(7) Peng, H. L.; Ran, C. B.; Yu, X. C.; Zhang, R.; Liu, Z. F. *Adv. Mater.* **2005**, *17*, 459−464.
(8) Nafady, A.; Bond, A. M.; Bilyk, A.; Harris, A. R.; Bhatt, A. I.; O'Mullane, A. P.; De Marco, R. *J. Am. Chem. Soc.* **2007**, *129*, 2369−2382.
(9) Cano, M.; Palenzuela, B.; Rodriguez-Amaro, R. *Electroanalysis* **2006**, *18*, 1068−1074.
(10) Llopis, X.; Merkoci, A.; del Valle, M.; Alegret, S. *Sens. Actuators, B* **2005**, *107*, 742−748.
(11) Pandey, P. C.; Upadhyay, S.; Sharma, S. *Electroanalysis* **2003**, *15*, 1115−1119.
(12) Yasuda, A.; Seto, J. *J. Electroanal. Chem.* **1988**, *247*, 193−202.
(13) Valade, L.; De Caro, D.; Malfant, I.; Ouahab, L.; Yagubskii, E. *NATO Sci. Ser., II* **2004**, *139*, 241−268.
(14) Nafady, A.; O'Mullane, A. P.; Bond, A. M.; Neufeld, A. K. *Chem. Mater.* **2006**, *18*, 437−4384.
(15) Onodera, T.; Matsuo, S.; Hiraishi, K.; Masuhara, A.; Kasai, H.; Oikawa, H. *CrystEngComm* **2012**, *14*, 7586−7589.
(16) Kotsiliou, A. M.; Risen, W. M. *Solid State Commun.* **1988**, *68*, 503−505.
(17) Lopez, N.; Zhao, H. H.; Prosvirin, A. V.; Wernsdorfer, W.; Dunbar, K. R. *Dalton Trans.* **2010**, *39*, 4341−4352.
(18) Ouyang, C. B.; Guo, Y. B.; Liu, H. B.; Zhao, Y. J.; Li, G. X.; Li, Y. J.; Song, Y. L.; Li, Y. L. *J. Phys. Chem. C* **2009**, *113*, 7044−7051.
(19) Hibbs, W.; Arif, A. M.; Botoshansky, M.; Kaftory, M.; Miller, J. S. *Inorg. Chem.* **2003**, *42*, 2311−2322.
(20) O'Kane, S. A.; Clerac, R.; Zhao, H. H.; Xiang, O. Y.; Galan-Mascaros, J. R.; Heintz, R.; Dunbar, K. R. *J. Solid State Chem.* **2000**, *152*, 159−173.
(21) Lopez, N.; Zhao, H. H.; Prosvirin, A. V.; Chouai, A.; Shatruk, M.; Dunbar, K. R. *Chem. Commun.* **2007**, 4611−4613.
(22) Potember, R. S.; Poehler, T. O.; Rappa, A.; Cowan, D. O.; Bloch, A. N. *Synth. Met.* **1982**, *4*, 371−380.
(23) Le, T. H.; Nafady, A.; Qu, X.; Martin, L. L.; Bond, A. M. *Anal. Chem.* **2011**, *83*, 6731−6737.
(24) Abrahams, B. F.; Elliott, R. W.; Hudson, T. A.; Robson, R. *Cryst. Growth Des.* **2013**, *13*, 3018−3027.
(25) Grossel, M. C.; Duke, A. J.; Hibbert, D. B.; Lewis, I. K.; Seddon, E. A.; Horton, P. N.; Weston, S. C. *Chem. Mater.* **2000**, *12*, 2319−2323.
(26) Suchanski, M. R.; Vanduyne, R. P. *J. Am. Chem. Soc.* **1976**, *98*, 250−252.

(27) Lombardo, A.; Fico, T. R. *J. Org. Chem.* **1979**, *44*, 209−212.
(28) Martin, E. L. U.S. Patent 3,558,671, 1971; p 3.
(29) Liang, H.-C.; Karlin, K. D.; Dyson, R.; Kaderli, S.; Jung, B.; Zuberbühler, A. D. *Inorg. Chem.* **2000**, *39*, 5884−5894.
(30) Le, T.; O'Mullane, A.; Martin, L.; Bond, A. *J. Solid State Chem.* **2011**, *15*, 2293−2304.
(31) Sheldrick, G. *Acta Crystallogr., Sect. A* **2008**, *64*, 112−122.
(32) Farrugia, L. *J. Appl. Crystallogr.* **1999**, *32*, 837−838.
(33) Le, T. H.; Nafady, A.; Lu, J.; Peleckis, G.; Bond, A. M.; Martin, L. L. *Eur. J. Inorg. Chem.* **2012**, 2889−2897.
(34) Bard, A. J.; Faulkner, L. R. *Electrochemical Methods: Fundamentals and Applications,* 2nd ed.; John Wiley & Sons, Inc.: New York, 2001.
(35) Harris, A. R.; Nafady, A.; O'Mullane, A. P.; Bond, A. M. *Chem. Mater.* **2007**, *19*, 5499−5509.
(36) Harris, A. R.; Neufeld, A. K.; O'Mullane, A. P.; Bond, A. M. *J. Mater. Chem.* **2006**, *16*, 4397−4406.
(37) Zanon, I.; Pecile, C. *J. Phys. Chem.* **1983**, *87*, 3657−3664.
(38) Dixon, D. A.; Calabrese, J. C.; Miller, J. S. *J. Phys. Chem.* **1989**, *93*, 2284−2291.
(39) Wang, X. T.; LiableSands, L. M.; Manson, J. L.; Rheingold, A. L.; Miller, J. S. *Chem. Commun.* **1996**, 1979−1980.
(40) Long, G.; Willett, R. D. *Inorg. Chim. Acta* **2001**, *313*, 1−14.
(41) Kamitsos, E. I.; Risen, W. M. *Solid State Commun.* **1983**, *45*, 165−169.
(42) Kamitsos, E. I.; Risen, W. M. *J. Chem. Phys.* **1983**, *79*, 5808−5819.
(43) Hoshino, H.; Matsushita, S.; Samura, H. *Jpn. J. Appl. Phys., Part 2* **1986**, *25*, L341−L342.
(44) Siedle, A. R.; Candela, G. A.; Finnegan, T. F. *Inorg. Chim. Acta* **1979**, *35*, 125−130.
(45) Perruchas, S.; Boubekeur, K. *Dalton Trans.* **2004**, 2394−2395.
(46) Harris, A. R.; Neufeld, A. K.; O'Mullane, A. P.; Bond, A. M.; Morrison, R. J. S. *J. Electrochem. Soc.* **2005**, *152*, C577−C583.
(47) Ke, J.; Su, W. T.; Howdle, S. M.; George, M. W.; Cook, D.; Perdjon-Abel, M.; Bartlett, P. N.; Zhang, W. J.; Cheng, F.; Levason, W.; Reid, G.; Hyde, J.; Wilson, J.; Smith, D. C.; Mallik, K.; Sazio, P. *Proc. Natl. Acad. Sci. U.S.A.* **2009**, *106*, 14768−14772.